Hydrometallurgy 187 (2019) 18–29

Contents lists available at ScienceDirect

Hydrometallurgy

journal homepage: www.elsevier.com/locate/hydromet

Catalytic mechanism of silver in the oxidative dissolution process of chalcopyrite: Experiment and DFT calculation

Hongbo Zhao[a,b,c], Yisheng Zhang[a,b], Menglin Sun[a,b], Pengfei Ou[d,*], Yanjun Zhang[a,b], Rui Liao[a,b], Guanzhou Qiu[a,b]

[a] School of Minerals Processing & Bioengineering, Central South University, Changsha, Hunan, China
[b] Key Lab of Bio-hydrometallurgy of Ministry of Education, Changsha, Hunan, China
[c] State Key Laboratory of Complex Nonferrous Metal Resources Clean Utilization, Kunming University of Science and Technology, China
[d] Department of Mining and Materials Engineering, McGill University, Montreal, Canada

ARTICLE INFO

Keywords:
Oxidative dissolution
Chalcopyrite
Catalytic mechanism
Silver
Sulfuric acid-ferric sulfate systems
Density functional theory calculations

ABSTRACT

In this work, combined techniques were utilized to interpret the catalytic mechanism of Ag^+ ions in sulfuric acid-ferric sulfate system of chalcopyrite. Density functional theory (DFT) calculations indicated the favorable adsorption of Ag^+ ions on reconstructed (001)-S and (112)-S surfaces of chalcopyrite, and confirmed the possibility of silver sulfide and sulfur vacancy formations. XPS analysis further indicated the formation of silver sulfide on chalcopyrite surface. Electrochemical analysis showed that silver catalyzed chalcopyrite dissolution by enhancing the electrochemical reactivity. In addition, the incorporation of silver atoms into the chalcopyrite surface might cause a major distortion in its structure and accelerated the diffusion rate of copper atoms mainly because of that the Cu^+ ionic radius is much smaller than that of Ag^+. As a consequence, the accumulation of passivating species was prevented and the adverse effect of passivation layer mainly consisting of polysulfide and metallic oxides was reduced, thus resulting in high dissolution kinetics. According to the present work, a model for interpreting catalytic mechanisms of Ag^+ in chalcopyrite dissolution is provided.

1. Introduction

The released acid and toxic metals during the oxidative dissolution of sulfide minerals can cause the acid mine drainage (AMD) (Thurston et al., 2010). The AMD with high concentrations of sulfuric acid and metal ions can severely contaminate water resource and soil (Johnson and Hallberg, 2005). Hence, the prevention of AMD formation and remediation of AMD sites are extremely important, which should be conducted based on the understanding of oxidative dissolution mechanism of sulfide minerals. There are varieties of sulfide minerals in the earth. Iron sulfides (including pyrite, arsenopyrite, chalcopyrite, bornite, and marmatite, etc) are the most common but other sulfide minerals can also produce AMD (Akcil and Koldas, 2006; Cheng et al., 2009). Silver is often contained in the sulfide minerals, and its role in the dissolution of sulfide minerals is extremely important. However, its role was rarely reported in the research field of AMD. Fe^{3+}/Fe^{2+} couple, oxygen, and bacteria played a major role of oxidants in accelerating the rate of acid and toxic metals ions releasing (Akcil and Koldas, 2006), which is similar to the hydrometallurgical systems of sulfide minerals.

Chalcopyrite ($CuFeS_2$) accounts for more than 70% of total copper reserves in the earth. It is also widely existed in solid wastes. The dissolution of chalcopyrite should be one of the origins of AMD. Chalcopyrite is mainly extracted through pyrometallurgy with high energy cost and serious environmental contamination. Many efforts have been made in developing an alternative hydrometallurgical technology to conventional pyrometallurgy, but chalcopyrite hydrometallurgy is still faced with a challenge of low dissolution kinetics (Klauber, 2008; Li et al., 2013; Watling, 2014; Zhao et al., 2019).

Silver ion (Ag^+) has been widely used as an important and versatile catalyst for a variety of organic synthesis reactions (Alvarez-Corral et al., 2008; Naodovic and Yamamoto, 2008; Weibel et al., 2008). It can also be used as a catalyst in inorganic reactions, for example, Ag^+ has been reported with remarkable catalysis in hydrometallurgical process of sulfide minerals and secondary resources, especially in copper hydrometallurgy (Ahonen and Tuovinen, 1990b; Chen and Lin, 2009; Deng and Liao, 2002; Gomez et al., 1999; Guo et al., 2011; Nazari et al., 2012a; Tapera et al., 2018; Wang et al., 2017). Ag^+ has been found to be an effective catalyst in chalcopyrite hydrometallurgy and the dissolution kinetics of chalcopyrite in the presence of Ag^+ can be

* Corresponding author.
E-mail address: pengfei.ou@mail.mcgill.ca (P. Ou).

https://doi.org/10.1016/j.hydromet.2019.05.002
Received 26 November 2018; Received in revised form 23 April 2019; Accepted 5 May 2019
Available online 06 May 2019
0304-386X/

remarkably accelerated (Ahonen and Tuovinen, 1990b; Gomez et al., 1999; Hiroyoshi et al., 2002; Nazari et al., 2012a; Zhao et al., 2017). However, the industrial application of silver catalyzed hydrometallurgy is still restricted mainly due to the high price of silver and difficulties in recovering catalyst effectively from residues.

To provide strategies for developing an alternative catalyst, optimizing the silver catalyzed process and recycling the catalyst effectively, the detailed catalysis mechanism of silver in chalcopyrite hydrometallurgy should be firstly illuminated. The catalytic mechanism of Ag^+ in chalcopyrite hydrometallurgy is complicated and is still in debate. The catalytic effect can be mainly attributed to the silver-containing intermediate species which was likely to be Ag_2S, metallic silver or others, but the specific species is still not certain. There are also debates about the role of silver-containing intermediate species. Previous studies proposed that the intermediate species accelerated chalcopyrite dissolution mainly by changing the morphology of elemental sulfur layer (Miller and Portillo, 1979; Price and Warren, 1986), increasing the conductivity of elemental sulfur layer (Munoz et al., 1998; Nazari et al., 2012a) and by forming $CuFeS_2$-Ag_2S galvanic couple (Ahonen and Tuovinen, 1990a; Córdoba et al., 2008b). Hiroyoshi et al. (Hiroyoshi et al., 2002) proposed that Ag_2S accelerated the transformation of chalcopyrite to Cu_2S which can be rapidly oxidized, thus accelerating chalcopyrite dissolution. Ghahremaninezhad et al. (Ghahremaninezhad et al., 2015) proposed that the formation of each Ag_2S molecule created a sulfur vacancy and a pair of holes in the passivation layer, thus accelerating chalcopyrite dissolution. In addition, the forming process of silver-containing intermediate species is still unknown. Some previous work proposed that it may form through the reactions between chalcopyrite and Ag^+ (Miller and Portillo, 1979; Wang et al., 2004), and some publications attributed it to the reactions between silver and elemental sulfur on chalcopyrite surface (Nazari et al., 2012a; Nazari et al., 2012b). Hiroyoshi et al. (Hiroyoshi et al., 2002) proposed that Ag_2S was produced through the reactions between Ag^+ and H_2S. Hence, it is vital to illuminate the detailed forming process of silver containing intermediate species and its role in the catalytic process.

Numerous hydrometallurgical systems for processing chalcopyrite have been reported, mainly including sulfuric acid-ferric sulfate, sulfuric acid-alternative oxidants, hybrid sulfate-chloride, hybrid sulfate-nitrate, acidic chloride, hybrid chloride-sulfate, and acidic chloride system, etc. Among them, sulfuric acid-ferric sulfate system with ferric ions (Fe^{3+}) as leaching agent is considered as the most promising alternative technology due to a number of environmental and economic advantages (Watling, 2013; Watling, 2014). Ferric leaching and biohydrometallurgy (bioleaching) technology are the most representative sulfuric acid-ferric sulfate systems. It is also similar to the aqueous chemistry conditions of AMD sites (Akcil and Koldas, 2006; Edwards et al., 2000).

Therefore, combined techniques were utilized to interpret the catalytic mechanism of Ag^+ in sulfuric acid-ferric sulfate system of chalcopyrite. The obtained results will provide guidance for developing new catalyst, optimizing the silver catalyzed hydrometallurgical process of chalcopyrite and for recycling the catalyst effectively. It would provide reference for the other metal ions catalyzed hydrometallurgical systems. In addition, the present study would also be useful in providing prevention and remediation strategies for AMD sites.

2. Experimental and computational methods

2.1. Dissolution experiments

Chalcopyrite samples of high purity were obtained from the geological museum of the Guangxi Province of China and were carefully selected. Mineralogical analysis proved that they were of extremely high purity without impurity, and it contained approximately 34.5% Cu, 31.5% Fe, and 33.1% S (wt%). Ore samples were ground by a ceramic ball mill and were then sieved through a 200-mesh sieve. Finally, all of the undersize products (-0.074 mm) were used for the dissolution experiments. In the dissolution experiments, 2 g of chalcopyrite and 100 mL of diluted sulfuric acid solution were added to separate 250 mL-shake flasks, which were placed in an orbital shaker with a temperature of 45 °C and rotating speed of 170 rpm. Ag_2SO_4 solution containing 1000 ppm Ag^{2+} was prepared in advance using deionized water, and then the utilized 2 ppm Ag^{2+} was obtained by adding 0.2 mL of the Ag_2SO_4 solution to the corresponding flasks. *Leptospirillum ferriphilum* (*L. ferriphilum*) (CCTC AB 206239) was obtained from the Key Lab of Bio-hydrometallurgy of Ministry of Education, Central South University, Changsha, China. Microbial culture and bioleaching experiments were conducted according to the previous publication (Zhao et al., 2015). During the whole dissolution process, pH was maintained around 1.70 with sulfuric acid, and the evaporative water was supplemented regularly with deionized water. Cupric and total iron concentrations were analyzed periodically by an inductively coupled plasma optical emission spectrometry (ICP-OES) (ICAP 7400, Thermo Fisher Scientific Co.). The redox potentials and pH values of solution were detected by ORP meter (BPP-922) and pH meter (PHSJ-4A). The mineralogical compositions of solid samples dissolved under different conditions were analyzed by synchrotron radiation-based X-ray diffraction (SR-XRD) at beamline 4B9A in Beijing Synchrotron Radiation Facility (BSRF) in Beijing, China.

2.2. Analytic techniques

Electrochemical experiments of open circuit potential (), electrochemical impedance spectroscopy (EIS), Tafel and cyclic voltammetry (CV) were conducted at the Princeton Model 283 potentiostat (EG&G of Princeton Applied Research). In the electrochemical experiments, a conventional three-electrode system consisting of a working electrode of chalcopyrite, a graphite rod being the counter electrode and a Ag/AgCl (3.0 M KCl) electrode being the reference electrode was used. The electrochemical experiments were all conducted in the electrolyte of dilute sulfuric acid (pH 1.70) and in the atmosphere of N_2. X-ray photoelectron spectroscopy (XPS) analysis was conducted by the model ESCALAB 250Xi. Spectra were recorded at constant pass energy of 20 eV and 0.1 eV/step using an Al K_α X-ray source.

2.3. Density functional theory (DFT) calculations

The relaxation and total energy calculations based on density functional theory (DFT) (Hohenberg and Kohn, 1964; Kohn and Sham, 1965) have been performed by using the plane-wave based Vienna ab-initio simulation package (VASP) (Kresse and Furthmüller, 1996). The generalized gradient approximation (GGA) parametrized by Perdew-Burke-Ernzerhof (PBE) (Perdew et al., 1996) was used to treat the exchange-correlation effects. The interactions between atomic cores and electrons were represented through the projector augmented-wave (PAW) method of Blöchl (Blöchl, 1994; Kresse and Joubert, 1999) as implemented in VASP. The optimized cut-off energy of 400 eV was adopted throughout, which was found sufficient in the optimization of slab models. In geometry optimizations, the total energy was converged to 10^{-5} eV, and forces acting on ions were required to be less than 0.02 eV/Å. A spin-polarization correction was addressed in our calculations.

To simulate the sulfur-terminated $CuFeS_2$ (001) and (112) surfaces (labeled as (001)-S and (112)-S), we used supercell models containing a 2×2 (001)-S and 2×1 (112)-S slabs with eight atomic layers, which were sufficient for the consideration of calculated surface and adsorption properties. A vacuum layer of 15 Å along the vertical direction perpendicular to the surface was employed to avoid spurious interactions between two adjacent slabs. In the calculations of the adsorbate adsorption and diffusion, the four uppermost surface layers were allowed to relax fully, while the remaining layers were fixed at the

optimized bulk positions. The atomic positions were relaxed using a conjugate-gradient algorithm during geometry optimization. The Brillouin zone integrations were performed using Monkhorst-Pack scheme (Monkhorst and Pack, 1976) with a 3 × 3 × 1 *k*-point grids for both the (001)-S and (112)-S surfaces, applying a generalized Gaussian smearing method with the smearing width set to 0.1 eV.

3. Results and discussions

3.1. Dissolution experiments

Fe^{3+} is the main oxidant in sulfuric acid-ferric sulfate system of chalcopyrite, and redox potential mainly determined by Fe^{3+}/Fe^{2+} ratio can reflect the oxidative atmosphere of the chosen system. The dissolution process of chalcopyrite in sulfuric acid-ferric sulfate system is significantly dependent on redox potential (Córdoba et al., 2008a; Hiroyoshi et al., 2008; Petersen and Dixon, 2006; Sandström et al., 2005). Hence, experiments of chalcopyrite dissolution by different Fe^{3+}/Fe^{2+} ratios in the presence or absence of Ag^+ were conducted to investigate the catalytic mechanism of silver in the dissolution process of chalcopyrite.

Fig. 1a shows that the dissolution kinetics of Cu was extremely slow without Fe^{3+}/Fe^{2+} redox couple, and no significant catalytic effect of Ag^+ can be found under this condition. The dissolution kinetics of Cu from chalcopyrite can be enhanced with the addition of Fe^{3+}/Fe^{2+} redox couple, and obvious catalytic effect of Ag^+ occurred in the presence of Fe^{3+}/Fe^{2+} redox couple. Fig. 1b indicates that Ag^+ cannot accelerate the dissolution of Fe from chalcopyrite in sulfuric acid-ferric sulfate system whether adding Fe^{3+}/Fe^{2+} redox couple or not. In addition, the dissolution behavior of chalcopyrite in the microbial system is similar with that of chalcopyrite in the presence of Fe^{3+}/Fe^{2+} redox couple because of that iron-oxidizing microorganism of L. *ferriphilum* can continuously oxidize Fe(II) to Fe (III), thereby providing Fe^{3+}/Fe^{2+} redox couple in the microbial system. Hence, Ag^+ can significantly catalyze the dissolution of Cu from chalcopyrite on the premise of adding Fe^{3+}/Fe^{2+} redox couple. However, the dissolution of Fe from chalcopyrite cannot be catalyzed by Ag^+ in sulfuric acid-ferric sulfate system. The hydrometallurgical process of chalcopyrite is dependent on redox potential because of that the oxidative dissolution of chalcopyrite contains a series of oxidation-reduction reactions. Fig. 1c indicates that the addition of Fe^{3+}/Fe^{2+} redox couple remarkably increased the redox potential of dissolution system. The redox potential of dissolution system was mainly determined by Fe^{3+}/Fe^{2+} ratio, and it was almost not affected by Ag^+. Hence, the catalytic effect of Ag^+ may not be attributed to controlling redox potential. Hiroyoshi et al. (Hiroyoshi et al., 2002) proposed that chalcopyrite was initially transformed to Cu_2S which can be dissolved rapidly in an appropriate range of redox potential, thus resulting in high copper extraction. The reaction between Ag^+ and H_2S speeded up the reaction of Cu_2S formation through Eq. (1) and Eq. (2), thus expediting chalcopyrite dissolution. What is

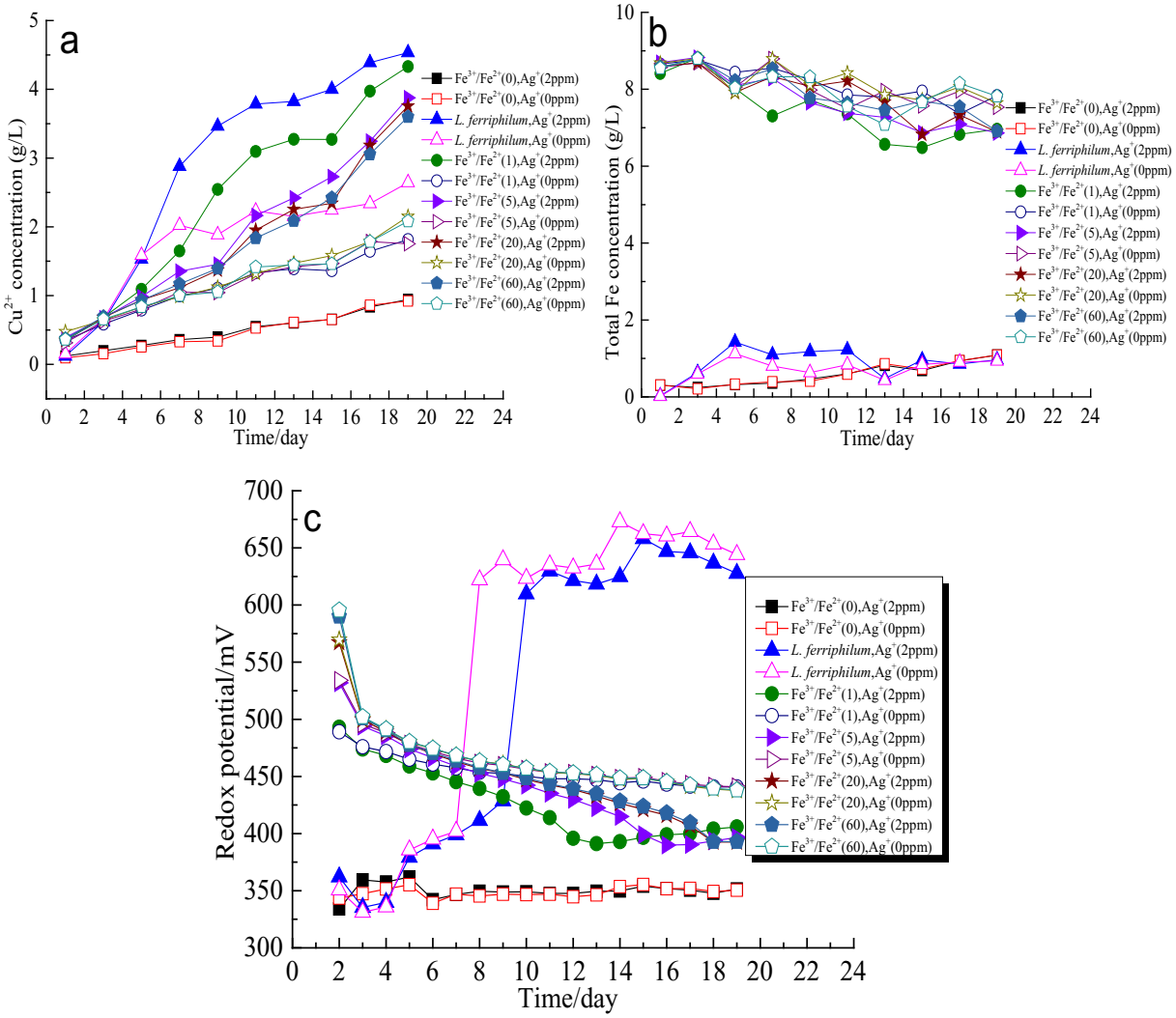

Fig. 1. The dissolution behaviors of chalcopyrite under different conditions: (a) Cu^{2+} concentration; (b) Total Fe concentration; (c) Redox potential.

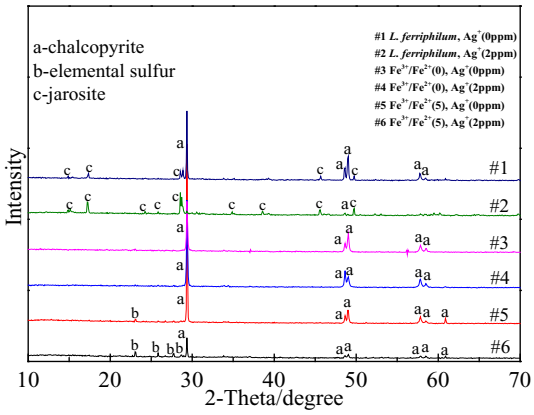

Fig. 2. SR-XRD of chalcopyrite samples dissolved for 20 days under different conditions.

more, it should be noted that Ag^+ may catalyze chalcopyrite dissolution mainly through changing the structures or properties of chalcopyrite surface.

$$2CuFeS_2 + 6H^+ + 2e^- \rightarrow Cu_2S + 2Fe^{2+} + 3H_2S \quad (1)$$

$$2Ag^+ + H_2S \rightarrow Ag_2S + 2H^+ \quad (2)$$

The SR-XRD of chalcopyrite samples dissolved for 20 days under different conditions is provided in Fig. 2. It can be found that a large amount of jarosite and elemental sulfur were produced when with the addition of Fe^{3+}/Fe^{2+} redox couple, the addition of Ag^+ even accelerated the production of jarosite and elemental sulfur. By contrast, the dissolution kinetics of chalcopyrite was the slowest when in the absence of Fe^{3+}/Fe^{2+} redox couple, but no significant amount of jarosite and elemental sulfur were detected in the dissolved chalcopyrite samples, indicating that jarosite and elemental sulfur may not be the main passivating species in sulfuric acid-ferric sulfate system of chalcopyrite. Even though the passivation mechanism and the specific passivating species in dissolution process of chalcopyrite are still in debate (Klauber, 2008), there was no doubt that the produced jarosite and elemental sulfur did not significantly hinder the dissolution of chalcopyrite when in the presence of Ag^+. In other words, the catalytic effect of Ag^+ overcame the adverse effects of passivating species. Hence, it is very likely that Ag^+ had changed the structures and properties of chalcopyrite surface, thus resulting in preventing passivation. To investigate the catalytic effects of Ag^+ on the structures and properties of chalcopyrite surface, electrochemical test, XPS analysis, and theoretical calculation were combined.

3.2. DFT calculations on the catalytic mechanism of Ag^+

In order to determine the exact reaction pathways for the catalytic mechanism of Ag^+ in chalcopyrite dissolution, firstly the adsorption of Ag^+ ions on the reconstructed (001)-S and (112)-S surfaces of chalcopyrite was studied by DFT calculations. In the following discussion, the high symmetry positions in the topmost two layers that exposed to the surface were chosen as the potential adsorption active sites. Several typical configurations were optimized by considering different initial orientations of adsorbate, in which the Ag^+ adsorbs on the top of Cu, Fe or S atoms, in the hollow sites, and above the centers of Cu—S and Fe—S bonds (as shown in Fig. 3). Generally, the adsorption energy is considered as a measure of the strength of substrate-adsorbate interaction. As the following, the adsorption energy E_{ads} calculated in the present work is defined as Eq. (3):

$$E_{ads} = E(\text{slab} + \text{adsorbate}) - E(\text{slab}) - E(\text{adsorbate}) \quad (3)$$

in which, the E(slab + adsorbate) is the calculated total energy of surface with adsorbed Ag^+ on it, E(slab) and E(adsorbate) are the calculated energies of clean surface and isolated Ag^+ ion, respectively. Accordingly, a negative E_{ads} value corresponds to a stable interaction system, the more negative the energy is, the stronger the adsorption system.

For the Ag^+ ion adsorption, the optimized configurations are shown in Fig. 4, and the corresponding initial and final configurations and adsorption energies for all the possible adsorption sites are summarized in Table 1. In the case of (001)-S surface (cf. Fig. 4a and b), it can be found that the Ag^+ ion is coordinated in the Cu2Fe2 hollow site and break the S—S dimer (site 2 in the Fig. 3b) with the Ag—S bond length of 2.63 Å and S-Ag-S forms an angle of 176.9°. The adsorption energy was calculated to be −2.83 eV, which indicate that the adsorption of Ag^+ ion on the (001)-S surface is significantly energetically favorable. It is also interesting to note that, when the Ag^+ ion is adsorption on the S_Top1 site (site 7 in Fig. 3a), it will automatically move to the Cu2Fe2 hollow site and the adsorption energy is similar to that of Cu2Fe2 hollow site. In terms of the (112)-S surface, as shown in Fig. 4c and d, the Ag^+ ion tends to be adsorbed in the Cu2Fe1 hollow site (site 2 in Fig. 3c) with a smaller negative adsorption energy of −0.66 eV when compared to that of (001)-S surface, residing 1.05 Å higher than the top S plane. The Ag^+ ion connects with three neighboring S atoms with the bond lengths of 2.50, 2.51, and 2.55 Å, respectively. Considering the above results, we believe that the hollow site of chalcopyrite surface shows a significant adsorption interaction with Ag^+ ion.

Moreover, to gain insights into the Ag^+ ion catalysis of chalcopyrite dissolution at the molecular level, DFT calculations were also performed to understand the reaction energetics. As suggested in the previous study (Ghahremaninezhad et al., 2015), the catalytic mechanism of Ag^+ in chalcopyrite dissolution are considered through the following steps:

$$2Ag^+_{aq} \rightarrow 2Ag^+_{ad} \quad (4)$$

$$2Ag^+_{ad} + S_S \rightarrow 2Ag^{CuFeS_2}_{Cu} + V_S + S_S + 2h^+ \quad (5)$$

$$2Ag^{CuFeS_2}_{Cu} + V_S + S_S \rightarrow 2Ag^{CuFeS_2}_{Cu} + S_S + V_S \rightarrow Ag_2S + V_S \quad (6)$$

where $Ag_{aq}{}^+$ and $Ag_{ad}{}^+$ denote a silver ion in the solution and adsorbed on the surface of the chalcopyrite passive film, $Ag_{Cu}{}^{CuFeS_2}$ indicates a silver atom is adsorbed in a copper (or iron) vacancy in the chalcopyrite passive film, V_S is for a sulfur vacancy, S_S denotes a sulfur atom in a sulfur position in the $CuFeS_2$ structure, and h^+ refers to the positive charge carriers, i.e., holes. Reaction (4) describes the adsorption of Ag^+ ion onto the surface of chalcopyrite passive film, and reaction (5) expresses an electrochemical reaction of Ag_2S formation. The formation of Ag_2S molecule in reaction (6) will introduce a sulfur vacancy in the chalcopyrite film, and subsequently, the silver atoms and sulfur vacancies might diffuse into the passive film structure.

According to the reactions (4–6), the DFT calculated results for four different steps in the reaction mechanism on (001)-S and (112)-S surfaces are shown in Fig. 5a and b, respectively: denoted as 1st Ag^+ adsorption, 2nd Ag^+ adsorption (along with the formation of S vacancy on the chalcopyrite surface), Ag_2S formation, and Ag_2S diffusion (equivalent to diffusion of silver into the chalcopyrite passive film). On the (001)-S surface, the first step of 1st Ag^+ ion adsorption on the surface is highly exothermic with an energy change of −2.83 eV. The following reactions are consecutively endothermic reactions, 0.56 eV for 2nd Ag^+ adsorption, 0.29 eV for Ag_2S formation, and 1.19 eV being the rate-limiting step for Ag_2S diffusion, respectively. In contrast, on the (112)-S surface, the 1st Ag^+ ion adsorption is less energetically favorable with an energy release of 0.66 eV when compared with that of (001)-S surface. After the adsorption of 1st Ag^+ ion, the 2nd Ag^+ ion adsorption is an endothermic reaction with energy slightly increased by 0.19 eV, followed by an exothermic reaction of Ag_2S formation with a large energy drop of -1.63 eV. The last step of Ag_2S diffusion with the diffusion of an Ag^+ ion into the chalcopyrite film is highly endergonic with an energy change of 1.06 eV, which is the rate-limiting step for the

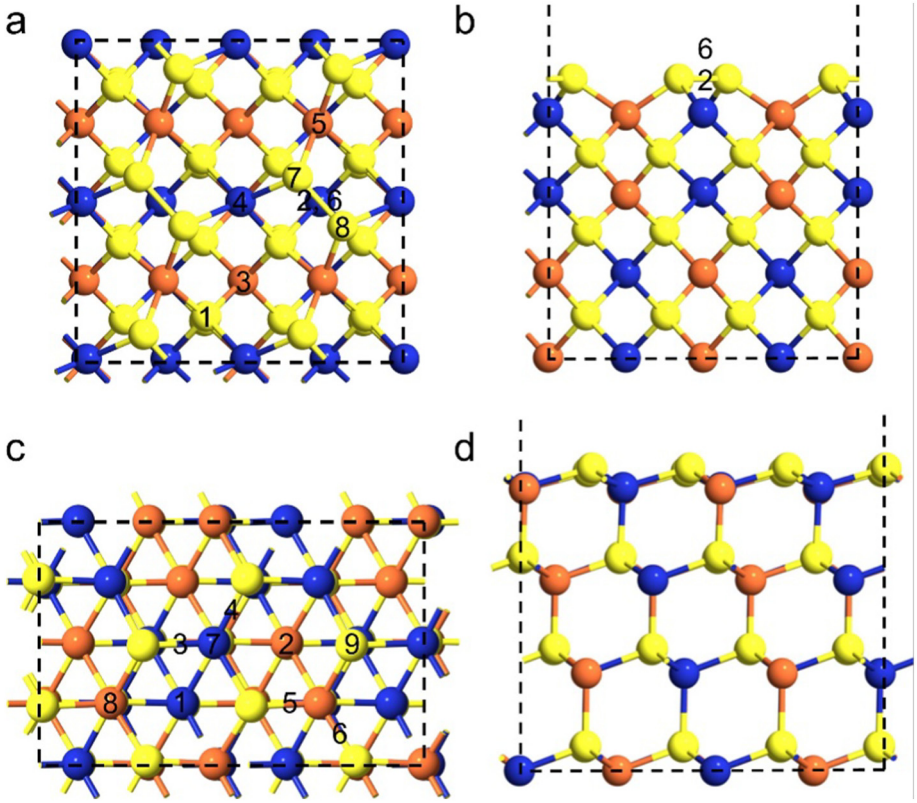

Fig. 3. Illustrations of various adsorption sites considered in the present study when determining the most stable configuration of the first Ag^+ ion adsorbed on the reconstructed (a, b)(001)-S and (c, d) (112)-S surfaces. For (001)-S surface, the 2 and 6 adsorption sites are overlapped in the top view. However, in the side view, 6 is at the top of a S—S bond, whereas 2 is in the hollow site which is made up of 2 copper atoms and 2 iron atoms. The orange, blue, and yellow balls represent iron, copper, and sulfur atoms, respectively. (For interpretation of the references to color in this figure legend, the reader is referred to the web version of this article.)

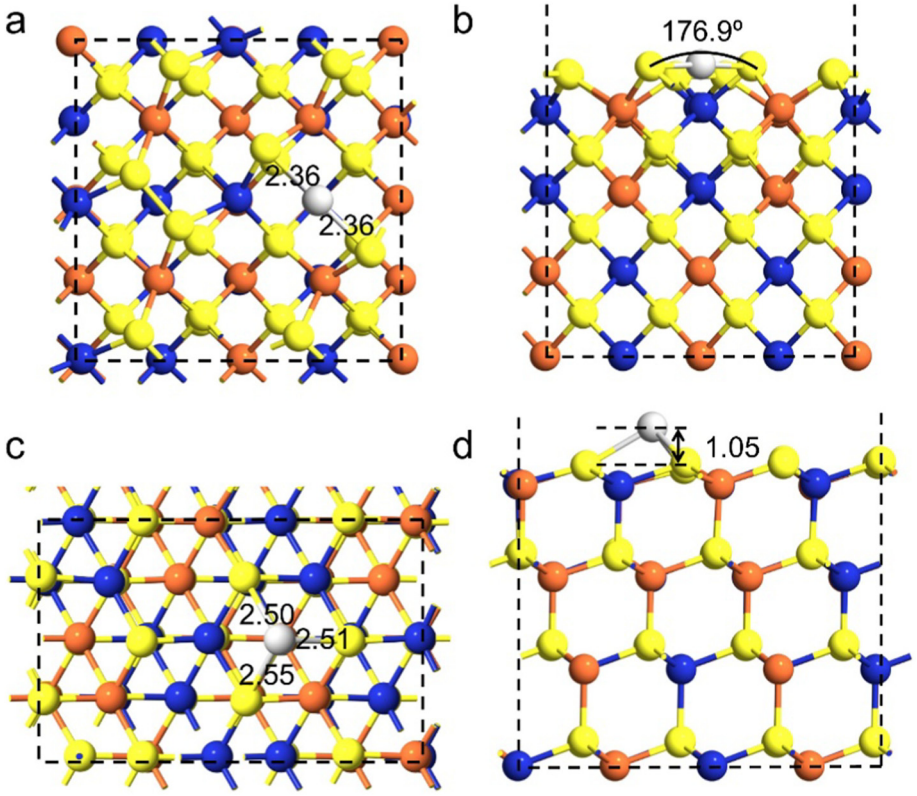

Fig. 4. Illustrations of the most stable adsorption site of the first Ag^+ ion adsorbed on the reconstructed (a, b) (001)-S and (c, d) (112)-S surfaces. The orange, blue, yellow, and light grey balls represent iron, copper, sulfur, and silver atoms, respectively. (For interpretation of the references to color in this figure legend, the reader is referred to the web version of this article.)

whole catalytic mechanism on (112)-S surface. From the calculation results, one can conclude that the energy diagram for Ag^+ ion catalysis of chalcopyrite dissolution on the (001)-S and (112)-S surfaces are different, but the last step of Ag^+ ion diffusion being the same rate-limiting step with similar energy barriers of 1.19 and 1.06 eV, respectively.

3.3. Surface species

To investigate the dissolution process of chalcopyrite under

Table 1
The initial and optimized final configurations (correspond to the adsorption sites denoted in Fig. 3) together with the DFT calculated adsorption energies (E_{ad}, in eV) of the first Ag^+ ion adsorbed on the reconstructed (001)-S and (112)-S surfaces.

Surface	No.	Initial	Final	E_{ad}
(001)-S	1	Cu2Fe2_Hollow1	-	−1.83
	2	**Cu2Fe2_Hollow2**	-	**−2.83**
	3	CuAgFe_Bridge	Moved to Cu2Fe2_Hollow1	−1.83
	4	S_Cu_S_Bridge	-	−1.69
	5	S_Fe_S_Bridge	-	−2.02
	6	S_S_Bridge	-	0.52
	7	S_Top1	Moved to Cu2Fe2_Hollow2	−2.79
	8	S_Top2	Moved to Cu2Fe2_Hollow1	−1.83
(112)-S	1	Cu1Fe2_Hollow	Formed an Ag—Fe bond	−0.47
	2	**Cu2Fe1_Hollow**	-	**−0.66**
	3	S_Cu_Bridge1	Moved to Cu_Top	−0.26
	4	S_Cu_Bridge2	Moved to Cu_Top	−0.05
	5	S_Fe_Bridge1	Partially moved to Cu2Fe1_Hollow	−0.25
	6	S_Fe_Bridge2	Moved to Cu1Fe2_Hollow	0.32
	7	Cu_Top	-	−0.05
	8	Fe_Top	-	−0.39
	9	S_Top	Partially moved to Cu2Fe1_Hollow	−0.25

The bold font indicates the energetically favorable adsorption configuration. Symbol "-" indicates the final configuration of Ag^+ ion adsorption remains the same as initial configuration.

different conditions,

the types and distributions of surface species of chalcopyrite electrode treated by different conditions were analyzed by using XPS. Fig. 6 shows that Cu, Fe, S and O containing species were the main surface species of chalcopyrite treated by air or H_2SO_4 without Ag^+. However, Ag containing species can be obviously detected on chalcopyrite surface treated by H_2SO_4 with Ag^+. Furtherly, the surface atomic percentages obtained by XPS surface survey analyses are shown in Table 2.

To further investigate the specific species of chalcopyrite surface under different conditions, the XPS spectra of Ag 3d, Cu 2p, Fe 2p, and Fe 3p were analyzed. The obtained XPS spectra were fitted by using the software of Thermo Avantage 5.52. During the fitting process, the binding energies of spectra were all referred to the C 1 s level at 284.8 eV, the background was achieved by using the Shirley method, and the spectra were fitted by the Gaussian-Lorentzian line (SGL) function (Shirley, 1972). Fig. 7a shows that the Ag $3d_{5/2}$ peak of chalcopyrite treated by Ag^+ was centered at 367.8 eV, which was similar to the binding energy of Ag—S species (Palacio et al., 2003). However, no significant Ag 3d peak can be detected in the other two chalcopyrite samples treated without Ag^+. Cu $2p_{3/2}$ peaks of chalcopyrite samples treated with no Ag^+ were both centered at about 932.0 eV, which were in accordance with the binding energy of Cu—S species of chalcopyrite, Cu_2S or CuS (Fujisawa et al., 1994; Nakai et al., 1978). However, the Cu 2p peaks of chalcopyrite treated by Ag^+ were remarkably weakened and almost disappeared. This may be caused by the high diffusion rate of copper atoms of chalcopyrite surface and by the coverage of formed silver sulfide. It can be found that the XPS spectra of Fe, especially Fe 3p peaks significantly shifted because of the treatment of Ag^+, indicating that the surrounding chemical environment of Fe atoms in the lattice structure of chalcopyrite surface was obviously changed because of the chemical reactions between Ag^+ and chalcopyrite. The obtained results further supported the results of theoretical calculations.

The S 2p spectra of chalcopyrite samples treated by different conditions were fitted using a 2:1 peak area ratio and 1.2 eV splitting for S $2p_{3/2}$ and S $2p_{1/2}$. It can be found that monosulfide (S^{2-}), disulfide (S_2^{2-}) and polysulfide (S_n^{2-}) were the main sulfur containing species of chalcopyrite surface treated by different conditions. The percentages of sulfur containing species on chalcopyrite surface after treating by different conditions were calculated from the peak area, which is shown

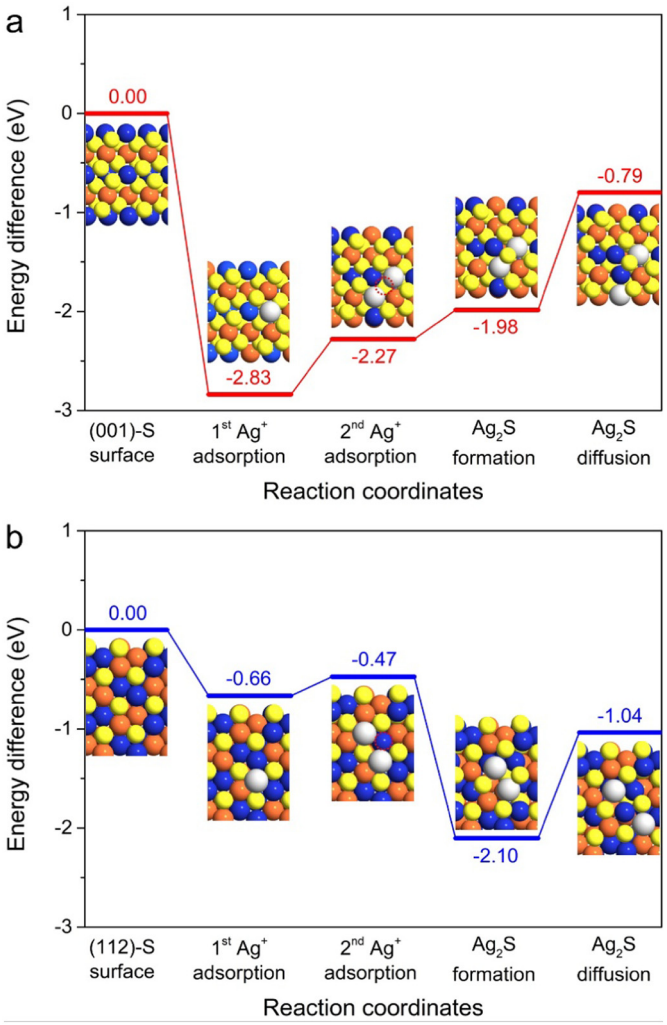

Fig. 5. DFT calculated energy difference and optimized configurations for the catalytic mechanism of Ag^+ in chalcopyrite dissolution on the reconstructed (a) (001)-S and (b) (112)-S surfaces, including four different steps: 1st Ag^+ adsorption, 2nd Ag^+ adsorption (along with the formation of S vacancy on the chalcopyrite surface), Ag_2S formation, and Ag_2S diffusion (equivalent to diffusion of silver into the chalcopyrite passive film). The orange, blue, yellow, and light grey spheres represent iron, copper, sulfur, and silver atoms, respectively. The sulfur vacancy is marked as a dashed red circle. (For interpretation of the references to color in this figure legend, the reader is referred to the web version of this article.)

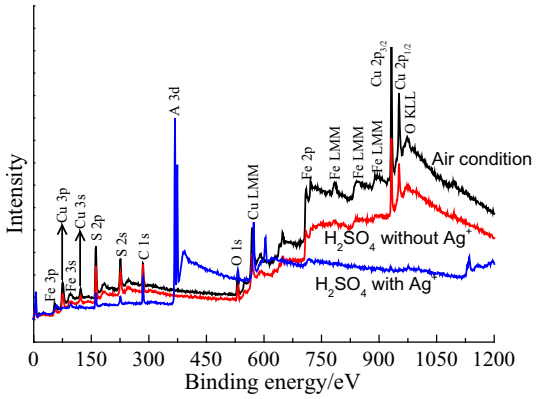

Fig. 6. Survey (full range) XPS spectra of chalcopyrite treated by different conditions.

Table 2
Surface atomic percentages.

Surface atomic percentages (%)	Cu	Fe	S	Ag	O
$H_2SO_4 + Ag^+$	2.38	1.21	31.72	49.58	15.11
H_2SO_4	26.97	11.31	47.48	–	14.24
Air	29.48	14.09	43.02	–	13.41

in Fig. 8d. Polysulfide has been previously reported as the surface species of chalcopyrite formed through surface reconstruction under air condition (Wang et al., 2016; Zhang et al., 2019). Some work proposed that a thin layer of polysulfide can be produced in the oxidative dissolution of chalcopyrite (Eq. (7)), the poorly reactive and relatively dense metal-deficient polysulfide with low conductivity and diffusion rate caused the passivation of chalcopyrite (Ammou-Chokroum et al., 1977; Hackl et al., 1995; Linge, 1976; Parker et al., 1981; Wang et al., 2016; Wang et al., 2017b; Yang et al., 2015). It can be found that a large amount of polysulfide was produced on chalcopyrite surface under the conditions of air or H_2SO_4. However, the percentage of polysulfide on chalcopyrite surface remarkably decreased due to the addition of Ag^+, indicating that Ag^+ prevented the accumulation of passivating species of polysulfide and then intensified chalcopyrite dissolution. It should be noted that the formation and coverage of silver sulfide may be one cause for the decrease of polysulfide percentage. To be exact, all the detected surfaces by XPS cannot be a simply chalcopyrite surface, it should be better described using the term of reaction surface which is the real region of the interfacial reactions.

$$CuFeS_2 \rightarrow Cu_{1-x}Fe_{1-y}S_{2-z} + xCu^{2+} + yFe^{2+} + zS^0 + 2(x+y)e^- \quad (7)$$

The XPS spectra of O 1 s peaks of chalcopyrite electrode treated by different conditions were provided in Fig. 9. The binding energy of O 1 s at 529.6 ± 0.1 eV, 531.5 ± 0.1 eV and 532.8 ± 0.1 eV can be mainly associated with O^{2-} in oxide phases, OH^- in hydroxide species and oxygen in sulfate (SO_4^{2-}) or/and water, respectively (Ghahremaninezhad et al., 2013). It can be found that O^{2-}, OH^- and SO_4^{2-} were the main oxygen containing species on chalcopyrite surface under the conditions of air or H_2SO_4. What is more, the percentage of hydroxide species on chalcopyrite in H_2SO_4 was higher than that in air, and the hydroxide species should be mainly attributed to FeOOH. However, almost no significant amount of O^{2-} species can be detected on chalcopyrite surface treated by Ag^+. O^{2-} species can be mainly assigned metallic oxides which were also considered as plausible passivating species in the dissolution process of chalcopyrite (similar with Eq. (8)) (Ahmadi et al., 2010; Khoshkhoo et al., 2014; Li and Huang, 2011). Hence, it can also be speculated that Ag^+ prevented the accumulation of passivating species of metallic oxides.

$$2CuFeS_2 + 5H_2O \rightarrow 2CuO + Fe_2O_3 + 4S^0 + 10H^+ + 10e^- \quad (8)$$

3.4. Surface properties

Cyclic voltammetry test can reveal the oxidation-reduction reactions of chalcopyrite at different applied potentials, so it can be used to interpret the thermodynamics and kinetics of the electrochemical dissolution process of chalcopyrite under different conditions. Fig. 10 presents the cyclic voltammetry curves of chalcopyrite electrode treated by different conditions. It can be found that the electrochemical dissolution processes of chalcopyrite under different conditions were similar, the addition of Ag^+ did not obviously change the dissolution mechanism of chalcopyrite. The first anodic peak mainly represents the direct oxidation of chalcopyrite to metal-deficient polysulfide (S_n^{2-}) (Eq. (7)). Many scholars have proposed that the formed poorly reactive and relatively dense metal-deficient polysulfide with low conductivity

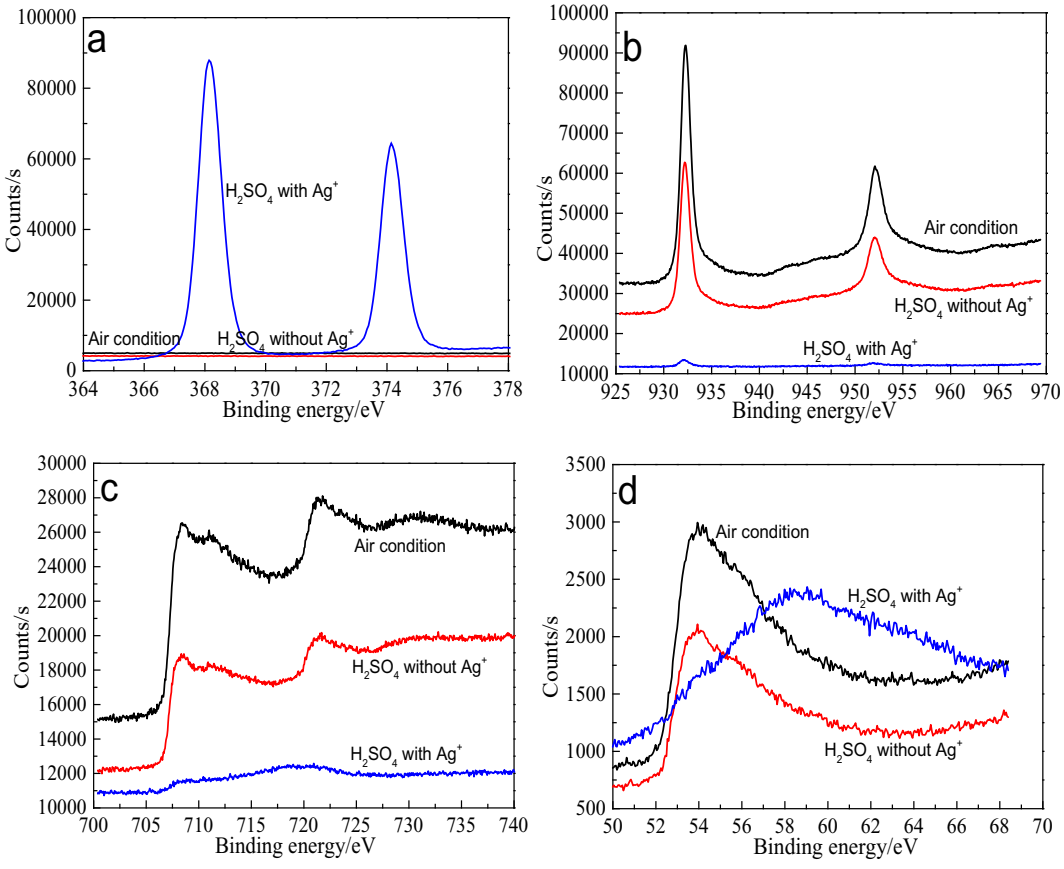

Fig. 7. XPS spectra of Ag 3d (a), Cu 2p (b), Fe 2p (c) and Fe 3p (d) of chalcopyrite treated by different conditions.

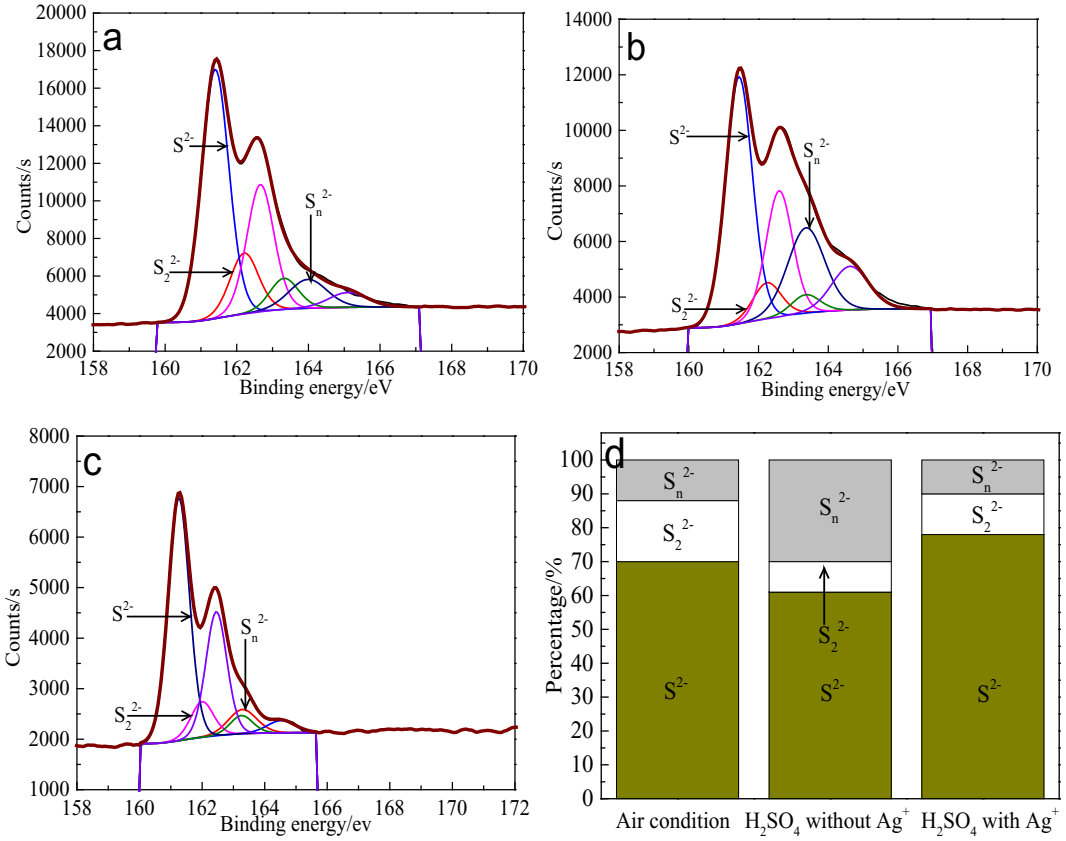

Fig. 8. S 2p spectra of chalcopyrite treated by different conditions: (a) air condition, (b) H_2SO_4 without Ag^+, (c) H_2SO_4 with Ag^+, (d) distribution of sulfur species on chalcopyrite surface.

and diffusion rate caused the passivation of chalcopyrite (Ammou-Chokroum et al., 1977; Hackl et al., 1995; Linge, 1976; Parker et al., 1981). The formed polysulfide was difficult to be directly oxidized by Fe^{3+} because of its relatively low oxidizing ability, so that stronger oxidants (such as potassium dichromate, nitric acid, etc.) were required to effectively dissolve it. The current density of peak a of chalcopyrite treated by sulfuric acid significantly decreased when compared with that of untreated chalcopyrite, indicating that the formed polysulfide obviously hindered the oxidative dissolution of chalcopyrite. However, the addition of Ag^+ significantly increased the current density of chalcopyrite, indicating that the addition of Ag^+ can accelerate the oxidative dissolution of chalcopyrite and reduce the passivation of polysulfide to a certain degree. The continuous anodic peaks of f, g and h represent the oxidative dissolution of Cu_2S. It can be found that the continuous peaks of g and h disappeared with the addition of Ag^+. One possible explanation may be that the addition of Ag^+ increased the electrochemical reactivity of chalcopyrite, thus leading to the direct oxidation of Cu_2S to CuS without the other intermediate reactions. Hence, the addition of Ag^+ did not significantly change the electrochemical dissolution mechanism of chalcopyrite but enhanced its electrochemical reactivity.

The value of open circuit potential (OCP) is a parameter reflecting the corrosion resistant abilities of materials. A lower value of OCP indicates that materials can be more easily to be corroded or oxidized. On the contrary, a higher value of OCP means that materials can be more difficult to be oxidized. Fig. 11a shows that the OCP of chalcopyrite treated by sulfuric acid remarkably increased compared with that of untreated chalcopyrite, indicating that it became more difficult to be oxidized. The formed passivation layer may be responsible for the high OCP. However, the addition of Ag^+ significantly decreased the OCP, indicating that the addition of Ag^+ reduced the adverse effect of passivation layer.

Tafel test can be used to analyze the corrosion kinetics of materials, parameters of oxidative corrosion potential (E_{corr}) and corrosion current density (I_{corr}) can be used to analyze the corrosion kinetics (Fig. 11b). The corrosion current density of chalcopyrite treated by sulfuric acid significantly decreased to about 0.478 μA/cm^2 compared with 2.234 μA/cm^2 of untreated chalcopyrite, indicating that the oxidative corrosion kinetics of chalcopyrite was slowed down because of passivation. However, the corrosion current density of chalcopyrite treated by Ag^+ was about 1.066 μA/cm^2 which was remarkably increased when compared with that of chalcopyrite treated by sole sulfuric acid (0.478 μA/cm^2), indicating that the oxidative corrosion kinetics of chalcopyrite was enhanced due to the addition of Ag^+. Hence, the addition of Ag^+ reduced the adverse effect of passivation layer through intensifying the oxidative corrosion kinetics.

Electrochemical impedance spectroscopy (EIS) can be used to analyze the kinetics model of charge transfer. The EIS spectra were fitted and analyzed, and the Nyquist impedance spectra and Bode plots are provided in Fig. 12 based on the proposed equivalent circuit. The well-fitted results of impedance parameters for the equivalent circuit are shown in Table 3. R_{sol} represents the solution resistance, R_1 means the charge transfer resistance and R_2 represents the passivation layer resistance. The charge transfer resistance can be shown as Eq. (9) (Ghahremaninezhad et al., 2012).

$$R_1 = \frac{RT}{nFi_0} \tag{9}$$

where the parameter of R, T, n and F represents the ideal gas constant (R = 8.314 J·K^{-1}·mol^{-1}), temperature (K), charge transfer number and Faraday constant (F = 96,494C), respectively. The value of i_0 represents the exchange current density of electrochemical reactions. A

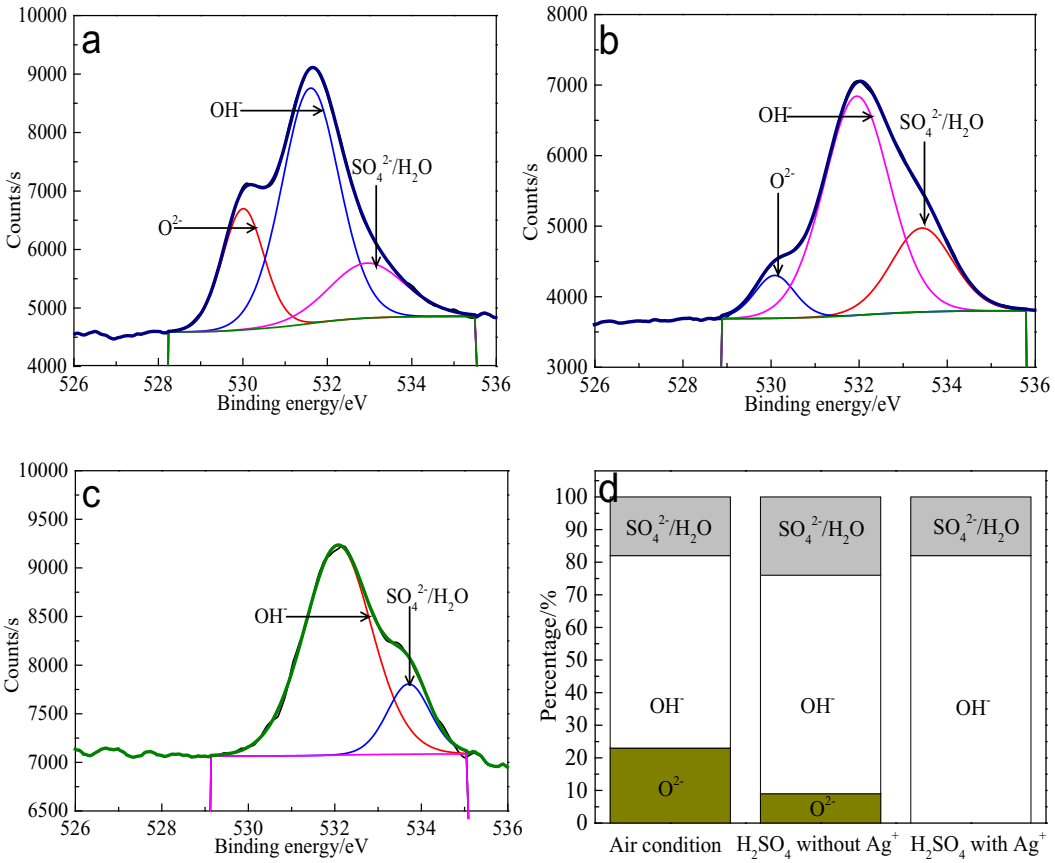

Fig. 9. O 1s spectra of chalcopyrite treated by different conditions: (a) air condition, (b) H_2SO_4 without Ag^+, (c) H_2SO_4 with Ag^+, (d) distribution of oxygen species on chalcopyrite surface.

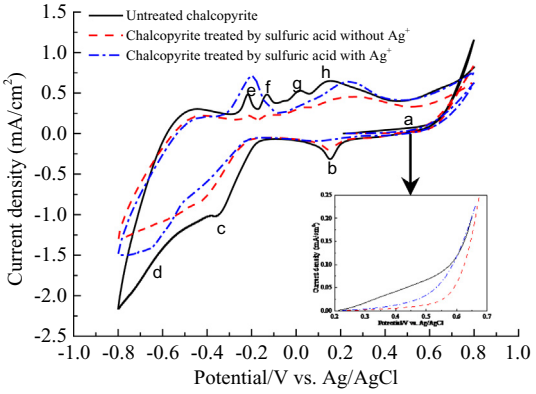

Fig. 10. Cyclic voltammetry curves of chalcopyrite electrode treated by different conditions (20 mV/s).

high value of i_0 and low value of R_1 indicate that the corresponding kinetics of electrochemical reactions was high, and vice versa. The charge transfer resistance of chalcopyrite treated by sulfuric acid remarkably increased compared with that of untreated chalcopyrite, indicating that the electrochemical reactions were hindered. However, the charge transfer resistance of chalcopyrite significantly decreased because of the Ag^+ addition. Similar results can be found in the parameters of passivation layer resistance (Table 3). The passivation layer resistance can be shown as Eq. (10).

$$R_2 = \frac{R_1^2\ |B|}{a - R_1\ |B|} \tag{10}$$

where the parameter of a is the charge transfer coefficient. The passivation layer resistance of chalcopyrite treated by sulfuric acid remarkably increased compared with that of untreated chalcopyrite, indicating that obvious passivation layer was formed on the chalcopyrite surface and further hindered the electrochemical reactions. The addition of Ag^+ decreased the passivation layer resistance of chalcopyrite when compared with that of chalcopyrite treated by sole sulfuric acid, indicating that the presence of Ag^+ reduced the adverse effect of passivation layer through decreasing the resistance and increasing the charge transfer rate.

3.5. Discussions on the catalytic mechanisms of Ag^+

From DFT calculations, the hollow site on the chalcopyrite surface shows a significant adsorption interaction with Ag^+ ion and formation of silver sulfide species, accompanied by the formation of sulfur vacancies. The sulfur vacancies formed in reaction (5) can be accountable for a high point defect concentration and result in high electrochemical reactivity. In addition, the sulfur vacancies is also responsible for the formation of chalcopyrite passive film covered with a porous surface layer, which has been validated by experimental observations (Ballester, 1987; Gomez et al., 1999; Muñoz et al., 2007; Sato et al., 2000; Wang et al., 2004; Yuehua et al., 2002). It is also confirmed that the formation of porous surface layer is a result of both a sufficiently high rate of vacancy generation and condensation of excess vacancies. It is also significant to point out that, the diffusion of silver atoms (equivalent to Ag_2S diffusion in Fig. 5a and b) into the chalcopyrite passive film also has a remarkable impact on the chalcopyrite dissolution. The diffusion of silver atoms into the chalcopyrite passive film may induce a significantly large lattice distortion due to a larger ionic radius of Ag^+ (129 pm) than that of Cu^+ (91 pm). Therefore, we would expect the diffusion kinetics of copper (and iron) atoms is accelerated in

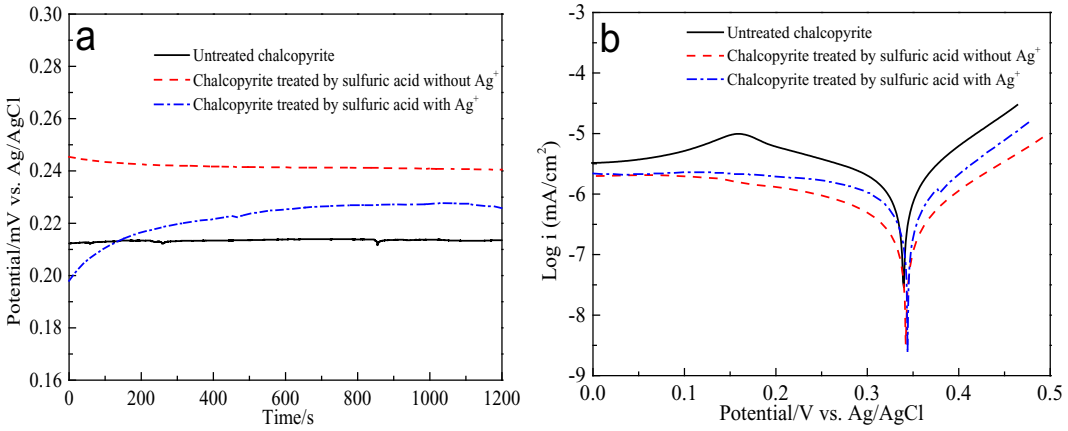

Fig. 11. Open circuit potential (a) and Tafel curves (b) of chalcopyrite electrode treated by different conditions.

the silver-incorporated chalcopyrite passive film than the one without silver-incorporation (Kadrgulov et al., 2001; Parker et al., 2003). XPS results of Cu 2p and Fe 3p (Fig. 7) and DFT calculations further supported the above conclusions. On the other hand, combined with the analytical results of XPS and electrochemistry, it can be speculated that Ag^+ prevented the accumulation of passivating species of polysulfide and metallic oxides mainly through accelerating its further oxidative dissolution process (Eqs. 7 and 8). As a consequence, the presence of Ag^+ ion enhanced the electrochemical reactivity of chalcopyrite through creating silver sulfide species and sulfur vacancy, and then prevented the accumulation of passivating species, thus resulting in high dissolution kinetics. According to the present work, a model for

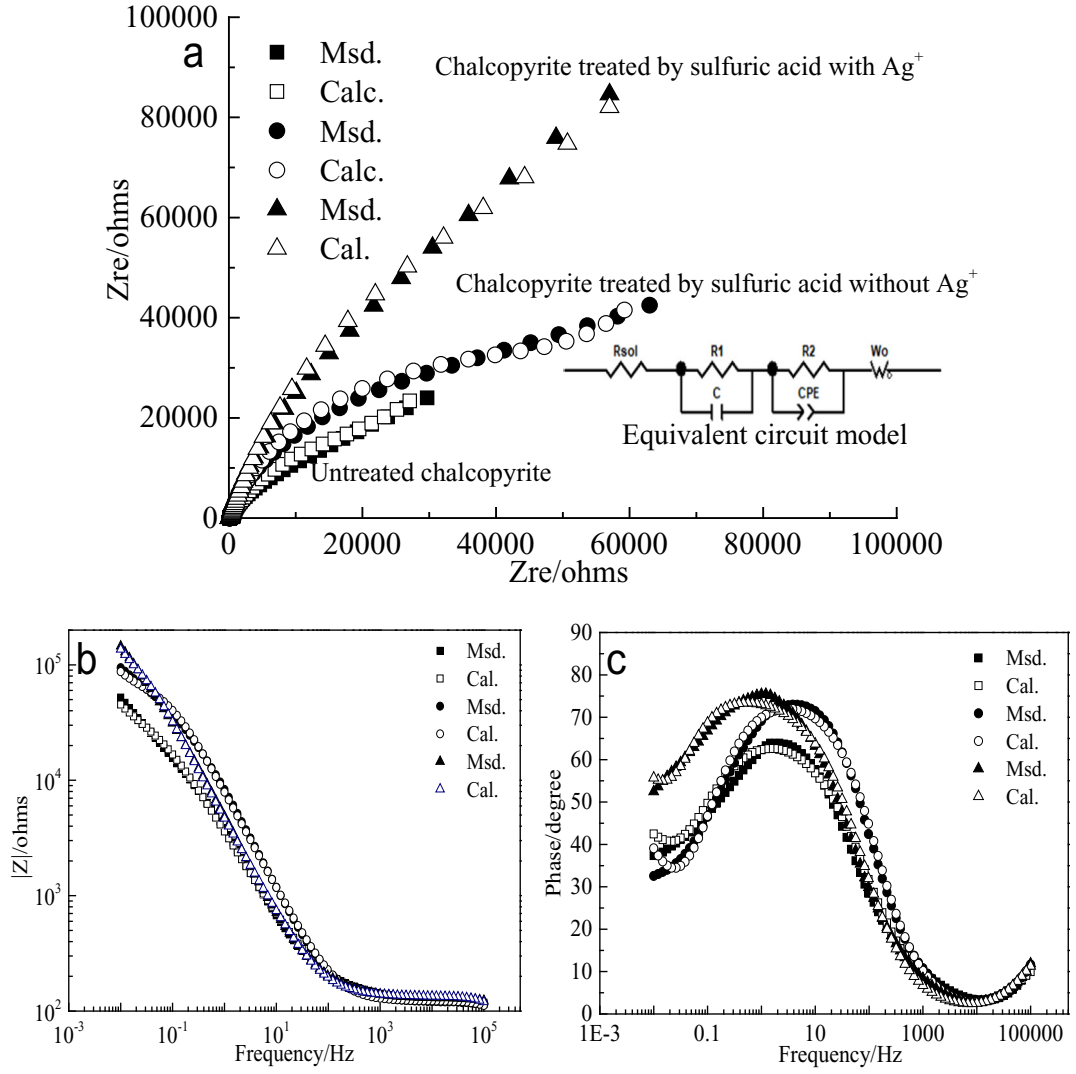

Fig. 12. Electrochemical impedance spectroscopy of chalcopyrite electrode treated by different conditions: (a) Nyquist impedance spectra; (b, c) Bode plots.

Table 3
Impedance parameters for the equivalent circuit.

Element	R_{sol} (Ω/cm^2)	R_1 (Ω/cm^2)	C (e^{-8}F/cm^2)	R_2 (Ω/cm^2)	CPE (Ss$^{1/2}$/cm^2)		W_o (Ss$^{1/2}$/cm^2)		
					CPE-T (e^{-5})	CPE-P	W_o-R (e^{-6})	W_o-T (e^{-12})	W_o-P
Untreated	87.68	40.1	2.98	20,034	12.0	0.81	99.9	3.86	0.34
H_2SO_4	69.59	52.22	1.67	54,195	3.04	0.86	7.61	5.97	0.40
H_2SO_4 + Ag^+	83.77	49.79	2.17	43,672	10.5	0.96	12.2	2.04	0.39

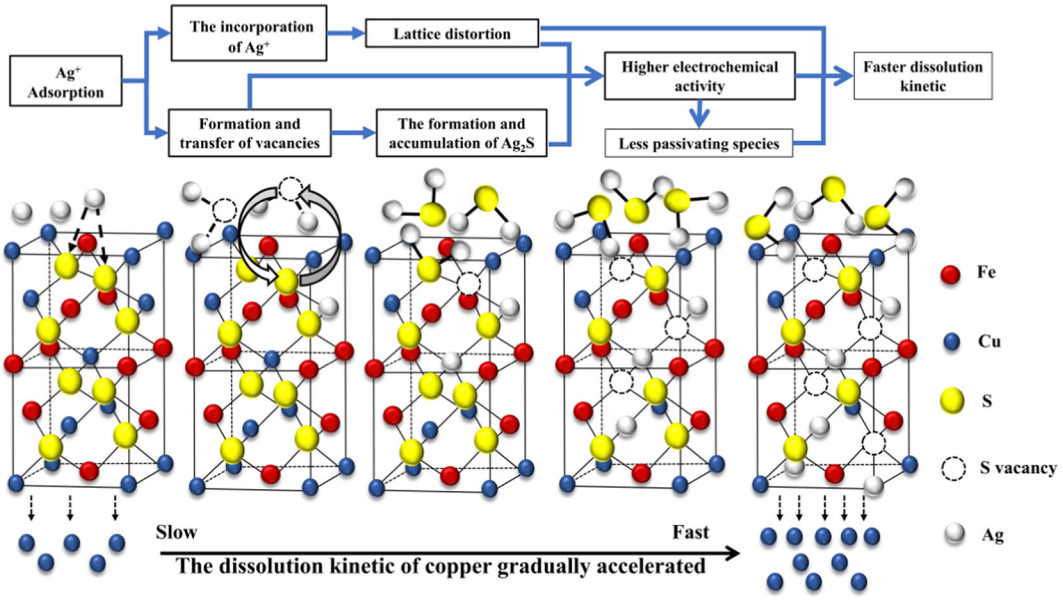

Fig. 13. A model for interpreting catalytic mechanisms of Ag^+ in chalcopyrite dissolution.

interpreting catalytic mechanisms of Ag^+ in chalcopyrite dissolution is provided in Fig. 13.

4. Conclusions

Ag^+ can remarkably catalyze the dissolution process of chalcopyrite in sulfuric acid-ferric sulfate system with necessary presence of oxidants. DFT calculations indicate that the Cu—Fe hollow site of chalcopyrite surface showed a significant adsorption interaction with Ag^+ ion and possible formation of silver sulfide species. In addition, the reaction energetics for Ag^+ ion catalysis of chalcopyrite dissolution on the (001)-S and (112)-S surfaces are different, but the last step of Ag^+ ion diffusion being the same rate-limiting step with similar energy barriers of 1.19 and 1.06 eV, respectively. The adsorption of Ag^+ produced sulfur vacancy and silver sulfides, which increased the electrochemical reactivity of chalcopyrite, such as low OCP, low resistance, and high corrosion current density value. As a consequence, the electrochemical reactions of chalcopyrite are enhanced and the production of passivation layer is slowed down, thus resulting in catalyzing the oxidative dissolution process of chalcopyrite.

Acknowledgements

This work was supported by the National Natural Science Foundation of China (51704331), Young Elite Scientists Sponsorship Program by CAST (2017QNRC001), Innovation-Driven Project of Central South University (2018CX019) and the Open Funds of Beijing Synchrotron Radiation Facility (No. 2017-BEPC-PT-000466).

References

Ahmadi, A., Schaffie, M., Manafi, Z., Ranjbar, M., 2010. Electrochemical bioleaching of high grade chalcopyrite flotation concentrates in a stirred bioreactor. Hydrometallurgy 104 (1), 99–105.
Ahonen, L., Tuovinen, O., 1990a. Silver catalysis of the bacterial leaching of chalcopyrite-containing ore material in column reactors. Miner. Eng. 3 (5), 437–445.
Ahonen, L., Tuovinen, O.H., 1990b. Catalytic effects of silver in the microbiological leaching of finely ground chalcopyrite-containing ore materials in shake flasks. Hydrometallurgy 24 (2), 219–236.
Akcil, A., Koldas, S., 2006. Acid Mine Drainage (AMD): causes, treatment and case studies. J. Clean. Prod. 14 (12), 1139–1145.
Alvarez-Corral, M., Munoz-Dorado, M., Rodriguez-Garcia, I., 2008. Silver-mediated synthesis of heterocycles. Chem. Rev. 108 (8), 3174–3198.
Ammou-Chokroum, M., Cambazoglu, M., Steinmez, D., 1977. Oxydation menagée de la chalcopyrite en solution acide: analyses cinétique de réactions. II. Modéles diffusionales. Bull. Soc. Fr. Miner. Cristallogr 100, 161–177.
Ballester, A., 1987. A study of the mechanism of silver-catalysed bioleaching of chalcopyrite. In: Separation Processes in Hydrometallurgy. Ellis Horwood Limited, pp. 99–110.
Blöchl, P.E., 1994. Projector augmented-wave method. Phys. Rev. B 50 (24), 17953.
Chen, S.Y., Lin, J.G., 2009. Enhancement of metal bioleaching from contaminated sediment using silver ion. J. Hazard. Mater. 161 (2), 893–899.
Cheng, H., Hu, Y., Luo, J., Xu, B., Zhao, J., 2009. Geochemical processes controlling fate and transport of arsenic in acid mine drainage (AMD) and natural systems. J. Hazard. Mater. 165 (1), 13–26.
Córdoba, E., Muñoz, J., Blázquez, M., González, F., Ballester, A., 2008a. Leaching of chalcopyrite with ferric ion. Part II: effect of redox potential. Hydrometallurgy 93 (3–4), 88–96.
Córdoba, E., Muñoz, J., Blázquez, M., González, F., Ballester, A., 2008b. Leaching of chalcopyrite with ferric ion. Part III: effect of redox potential on the silver-catalyzed process. Hydrometallurgy 93 (3), 97–105.
Deng, T., Liao, M., 2002. Gold recovery enhancement from a refractory flotation concentrate by sequential bioleaching and thiourea leach. Hydrometallurgy 63 (3), 249–255.
Edwards, K.J., Bond, P.L., Druschel, G.K., McGuire, M.M., Hamers, R.J., Banfield, J.F., 2000. Geochemical and biological aspects of sulfide mineral dissolution: lessons from Iron Mountain, California. Chem. Geol. 169 (3), 383–397.
Fujisawa, M., Suga, S., Mizokawa, T., Fujimori, A., Sato, K., 1994. Electronic structures of $CuFeS_2$ and $CuAl_{0.9}Fe_{0.1}S_2$ studied by electron and optical spectroscopies. Phys. Rev.

B 49 (11), 7155–7164.
Ghahremaninezhad, A., Dixon, D.G., Asselin, E., 2012. Kinetics of the ferric–ferrous couple on anodically passivated chalcopyrite ($CuFeS_2$) electrodes. Hydrometallurgy 125–126 (8), 42–49.
Ghahremaninezhad, A., Dixon, D.G., Asselin, E., 2013. Electrochemical and XPS analysis of chalcopyrite ($CuFeS_2$) dissolution in sulfuric acid solution. Electrochim. Acta 87 (1), 97–112.
Ghahremaninezhad, A., Radzinski, R., Gheorghiu, T., Dixon, D.G., Asselin, E., 2015. A model for silver ion catalysis of chalcopyrite ($CuFeS_2$) dissolution. Hydrometallurgy 155, 95–104.
Gomez, E., Ballester, A., Blazquez, M., Gonzalez, F., 1999. Silver-catalysed bioleaching of a chalcopyrite concentrate with mixed cultures of moderately thermophilic micro-organisms. Hydrometallurgy 51 (1), 37–46.
Guo, P., Zhang, G., Cao, J., Li, Y., Fang, Z., 2011. Catalytic effect of Ag^+ and Cu^{2+} on leaching realgar (As_2S_2). Hydrometallurgy 106 (1), 99–103.
Hackl, R.P., Dreisinger, D.B., Peters, E., King, J.A., 1995. Passivation of chalcopyrite during oxidative leaching in sulfate media. Hydrometallurgy 39 (1), 25–48.
Hiroyoshi, N., Arai, M., Miki, H., Tsunekawa, M., Hirajima, T., 2002. A new reaction model for the catalytic effect of silver ions on chalcopyrite leaching in sulfuric acid solutions. Hydrometallurgy 63 (3), 257–267.
Hiroyoshi, N., Tsunekawa, M., Okamoto, H., Nakayama, R., Kuroiwa, S., 2008. Improved chalcopyrite leaching through optimization of redox potential. Can. Metall. Q. 47 (3), 253–258.
Hohenberg, P., Kohn, W., 1964. Inhomogeneous electron gas. Phys. Rev. 136 (3B), B864.
Johnson, D.B., Hallberg, K.B., 2005. Acid mine drainage remediation options: a review. Sci. Total Environ. 338 (1), 3–14.
Kadrgulov, R., Yakshibaev, R., Khasanov, M., 2001. Phase relations, ionic transport and diffusion in the alloys of Cu_2S-Ag_2S mixed conductors. Ionics 7 (1–2), 156–160.
Khoshkhoo, M., Dopson, M., Shchukarev, A., Sandström, Å., 2014. Chalcopyrite leaching and bioleaching: an X-ray photoelectron spectroscopic (XPS) investigation on the nature of hindered dissolution. Hydrometallurgy 149, 220–227.
Klauber, C., 2008. A critical review of the surface chemistry of acidic ferric sulphate dissolution of chalcopyrite with regards to hindered dissolution. Int. J. Miner. Process. 86 (1), 1–17.
Kohn, W., Sham, L.J., 1965. Self-consistent equations including exchange and correlation effects. Phys. Rev. 140 (4A), A1133.
Kresse, G., Furthmüller, J., 1996. Efficient iterative schemes for ab initio total-energy calculations using a plane-wave basis set. Phys. Rev. B 54 (16), 11169.
Kresse, G., Joubert, D., 1999. From ultrasoft pseudopotentials to the projector augmented-wave method. Phys. Rev. B 59 (3), 1758.
Li, A., Huang, S., 2011. Comparison of the electrochemical mechanism of chalcopyrite dissolution in the absence or presence of *Sulfolobus metallicus* at 70 °C. Miner. Eng. 24 (13), 1520–1522.
Li, Y., Kawashima, N., Li, J., Chandra, A., Gerson, A.R., 2013. A review of the structure, and fundamental mechanisms and kinetics of the leaching of chalcopyrite. Adv. Colloid Interf. Sci. 197, 1–32.
Linge, H.G., 1976. A study of chalcopyrite dissolution in acidic ferric nitrate by potentiometric titration. Hydrometallurgy 2 (1), 51–64.
Miller, J., Portillo, H., 1979. Silver catalysis in ferric sulphate leaching of chalcopyrite. In: 13th International Mineral Processing Congress. Elsevier, Amsterdam, pp. 851–901.
Monkhorst, H.J., Pack, J.D., 1976. Special points for Brillouin-zone integrations. Phys. Rev. B 13 (12), 5188.
Munoz, J.A., Go, C., Ballester, A., Bla, M.L., Gonza, F., Figueroa, M., 1998. Electrochemical behaviour of chalcopyrite in the presence of silver and Sulfolobus bacteria. J. Appl. Electrochem. 28 (1), 49–56.
Muñoz, J., Dreisinger, D., Cooper, W., Young, S., 2007. Silver-catalyzed bioleaching of low-grade copper ores. Part II: stirred tank tests. Hydrometallurgy 88 (1–4), 19–34.
Nakai, I., Sugitani, Y., Nagashima, K., Niwa, Y., 1978. X-ray photoelectron spectroscopic study of copper minerals. J. Inorg. Nucl. Chem. 40 (5), 789–791.
Naodovic, M., Yamamoto, H., 2008. Asymmetric silver-catalyzed reactions. Chem. Rev. 108 (8), 3132–3148.
Nazari, G., Dixon, D., Dreisinger, D., 2012a. The mechanism of chalcopyrite leaching in the presence of silver-enhanced pyrite in the Galvanox™ process. Hydrometallurgy 113, 122–130.
Nazari, G., Dixon, D., Dreisinger, D., 2012b. The role of silver-enhanced pyrite in enhancing the electrical conductivity of sulfur product layer during chalcopyrite leaching in the Galvanox™ process. Hydrometallurgy 113, 177–184.
Palacio, C., Ocón, P., Herrasti, P., Díaz, D., Arranz, A., 2003. XPS and ARXPS study of silver underpotential deposition on platinum in acid solution. J. Electroanal. Chem. 545, 53–58.
Parker, A.J., Paul, R.L., Power, G.P., 1981. Electrochemistry of the oxidative leaching of copper from chalcopyrite. J. Electroanal. Chem. Interfacial Electrochem. 118, 305–316.
Parker, A., Klauber, C., Kougianos, A., Watling, H., Van Bronswijk, W., 2003. An X-ray photoelectron spectroscopy study of the mechanism of oxidative dissolution of chalcopyrite. Hydrometallurgy 71 (1–2), 265–276.
Perdew, J.P., Burke, K., Ernzerhof, M., 1996. Generalized gradient approximation made simple. Phys. Rev. Lett. 77 (18), 3865.
Petersen, J., Dixon, D.G., 2006. Competitive bioleaching of pyrite and chalcopyrite. Hydrometallurgy 83 (1), 40–49.
Price, D., Warren, G., 1986. The influence of silver ion on the electrochemical response of chalcopyrite and other mineral sulfide electrodes in sulfuric acid. Hydrometallurgy 15 (3), 303–324.
Sandström, Å., Shchukarev, A., Paul, J., 2005. XPS characterisation of chalcopyrite chemically and bio-leached at high and low redox potential. Miner. Eng. 18 (5), 505–515.
Sato, H., Nakazawa, H., Kudo, Y., 2000. Effect of silver chloride on the bioleaching of chalcopyrite concentrate. Int. J. Miner. Process. 59 (1), 17–24.
Shirley, D.A., 1972. High-resolution X-ray photoemission spectrum of the valence bands of gold. Phys. Rev. B 5 (12), 4709.
Tapera, T., Sheean, J., Nikoloski, A.N., 2018. The effect of silver on the acidic ferric sulfate leaching of primary copper sulfides under recycle solution conditions observed in heap leaching. Part 2: synergistic additives. Hydrometallurgy 179, 1–7.
Thurston, R.S., Mandernack, K.W., Shanks III, W.C., 2010. Laboratory chalcopyrite oxidation by Acidithiobacillus ferrooxidans: oxygen and sulfur isotope fractionation. Chem. Geol. 269 (3–4), 252–261.
Wang, M., Zhang, Y., Deng, T., Wang, K., 2004. Kinetic modeling for the bacterial leaching of chalcopyrite catalyzed by silver ions. Miner. Eng. 17 (7), 943–947.
Wang, J., Gan, X., Zhao, H., Hu, M., Li, K., Qin, W., Qiu, G., 2016. Dissolution and passivation mechanisms of chalcopyrite during bioleaching: DFT calculation, XPS and electrochemistry analysis. Miner. Eng. 98, 264–278.
Wang, J., Liao, R., Tao, L., Zhao, H., Zhai, R., Qin, W., Qiu, G., 2017. A comprehensive utilization of silver-bearing solid wastes in chalcopyrite bioleaching. Hydrometallurgy 169, 152–157.
Wang, X., et al., 2017b. Synergetic effect of pyrite on strengthening bornite bioleaching by Leptospirillum ferriphilum. Hydrometallurgy 176, 9–16.
Watling, H., 2013. Chalcopyrite hydrometallurgy at atmospheric pressure: 1. Review of acidic sulfate, sulfate–chloride and sulfate–nitrate process options. Hydrometallurgy 140, 163–180.
Watling, H., 2014. Chalcopyrite hydrometallurgy at atmospheric pressure: 2. Review of acidic chloride process options. Hydrometallurgy 146, 96–110.
Weibel, J.M., Blanc, A., Pale, P., 2008. Ag-mediated reactions: coupling and heterocyclization reactions. Chem. Rev. 108 (8), 3149–3173.
Yang, Y., Harmer, S., Chen, M., 2015. Synchrotron-based XPS and NEXAFS study of surface chemical species during electrochemical oxidation of chalcopyrite. Hydrometallurgy 156, 89–98.
Yuehua, H., Guanzhou, Q., Jun, W., Dianzuo, W., 2002. The effect of silver-bearing catalysts on bioleaching of chalcopyrite. Hydrometallurgy 64 (2), 81–88.
Zhang, Y., Zhao, G., Lv, X., Tian, Y., Yang, L., Zou, G., Ji, X., 2019. The exploration and size engineering from natural chalcopyrite to high-performance electrode materials for lithium-ion batteries. ACS Appl. Mater. Interfaces 11, 6154–6165.
Zhao, H., Wang, J., Gan, X., Hu, M., Zhang, E., Qin, W., Qiu, G., 2015. Cooperative bioleaching of chalcopyrite and silver-bearing tailing by mixed moderately thermophilic culture: an emphasis on the chalcopyrite dissolution with XPS and electrochemical analysis. Miner. Eng. 81, 29–39.
Zhao, H., Gan, X., Wang, J., Tao, L., Qin, W., Qiu, G., 2017. Stepwise bioleaching of Cu-Zn mixed ores with comprehensive utilization of silver-bearing solid waste through a new technique process. Hydrometallurgy 171, 374–386.
Zhao, H., et al., 2019. The dissolution and passivation mechanism of chalcopyrite in bioleaching: an overview. Miner. Eng. 136, 140–154.